IOPscience iopscience.iop.org

Home Search Collections Journals About Contact us My IOPscience

Optical absorption by a Landau-quantized two-dimensional electron gas with one-dimensional periodic delta -modulation

This article has been downloaded from IOPscience. Please scroll down to see the full text article.

1994 J. Phys.: Condens. Matter 6 9219

(http://iopscience.iop.org/0953-8984/6/43/020)

View the table of contents for this issue, or go to the journal homepage for more

Download details:
IP Address: 171.66.16.151
The article was downloaded on 12/05/2010 at 20:56

Please note that terms and conditions apply.

J. Phys.: Condens. Matter 6 (1994) 9219–9233. Printed in the UK

Optical absorption by a Landau-quantized two-dimensional electron gas with one-dimensional periodic δ-modulation

Danhong Huang†, Godfrey Gumbs‡¶, Vassilios Fessatidis§ and Norman J M Horing‖

† Department of Electrical and Computer Engineering, Wayne State University, Detroit, MI 48202, USA

‡ Department of Physics and Astronomy, Hunter College, City University of New York, 695 Park Avenue, New York, NY 10021, USA

§ Physics Department, Fordham University, Rose Hill Campus, 441 East Fordham Road, Bronx, NY 10458, USA

‖ Department of Physics and Engineering Physics, Stevens Institute of Technology, Castle Point on the Hudson, Hoboken, NJ 07030, USA

Received 4 May 1994, in final form 6 August 1994

Abstract. An exact numerical diagonalization technique is used to calculate the energy eigenstates of a Landau-quantized two-dimensional electron gas under a one-dimensional periodic δ-modulation. On the basis of these calculations, we develop a self-consistent field theory for the absorption coefficient in the mid-infrared frequency regime. An extensive investigation is carried out in which we find that the plasmon mode changes from a cyclotron mode when the modulation is weak to tunnelling-split modes for the intermediate modulation and finally to edge and 1D lattice magnetoplasmon modes when the modulation is strong. Our numerical results show that as the magnetic field decreases, there exists electron tunnelling. However, for strong magnetic fields, electron tunnelling is suppressed. This suppression of electron tunnelling is signalled by the crossover of two tunnelling-split modes into a cyclotron mode at strong magnetic fields. The eigenenergy of the edge mode oscillates with electron density, related to soft or hard potential walls from the modulation for which the electron stays in extended and localized states, respectively.

1. Introduction

Recent discoveries such as the integral and fractional quantum Hall effects [1, 2] in the two-dimensional (2D) Landau-quantized electron gas (EG), the quenching of the Hall effect in 2D antidot arrays [3, 4, 5], the commensurability oscillations in the longitudinal resistance within 2D quantum dot [6] and 1D quantum wire [7] arrays, the evolution of magnetoplasmon modes in 1D antiwire arrays [8], and the optical absorption by quantum wires [9] are examples of physical phenomena which have stimulated and led to further interest in the study of the optical and transport properties in systems of reduced dimensionality. Strong electrostatic periodic modulations and mutual Coulomb scattering have produced novel effects in the 2DEG subject to 1D [10] or 2D [11] potential modulation. The rapid advances in submicrometre lithographic technology have led to the introduction of in-plane confinement within the 2DEG and the construction of quantum wires with many electrons

¶ Also at: The Graduate School and University Center, City University of New York, 33 West 42 Street, New York, NY 10036, USA.

0953-8984/94/439219+15$19.50 © 1994 IOP Publishing Ltd

occupying discrete energy subbands. The existence of a strong spatially modulated potential produces dramatic commensurability effects in the electron motion at low temperatures when a uniform external magnetic field is applied. In this type of artificial 1D potential array, many pronounced and intriguing features were observed in the magnetoresistance. For the weak-modulation limit, Gerhardts *et al* [12] and Vasilopoulos *et al* [13] presented calculations for the magnetoresistance of a 1D array of quantum wires. Appreciable commensurability oscillations were obtained in the longitudinal resistance caused by a lifting of the Landau-level degeneracy which leads to the formation of Landau bands in the presence of 1D potential modulation. When the electron motion is commensurate with the lattice, the electronic states are further modified into corresponding localized and extended states for specific strengths of the magnetic field. Instead of considering the usual weak-modulation limit, Wulf *et al* [10] calculated the band part of the Hall conductivity in the strong-modulation regime where giant oscillations were predicted. On the other hand, Cui *et al* [14] calculated the optically excited magnetoplasmon spectrum in the limit of weak 1D lateral modulation, in which commensurability oscillations as a function of the magnetic field were predicted.

Although there have been many experimental and theoretical studies of the optical and transport properties in 1D arrays of quantum wires, several subtle questions still remain to be resolved. The microphysics of this system in the weak-modulation limit can be studied with the use of a naive model based on first-order perturbation theory. In the strong-modulation limit, this system can be considered as a 1D lattice because the small effects from Landau quantization at weak magnetic fields are only expected to play a minor role. In the intermediate-modulation regime, the Landau and size quantization effects become comparable to each other. However, when perturbation theory is applied to the weak-modulation limit, the rich microphysics hidden in the large intermediate-modulation regime cannot be accounted for or understood.

This paper provides a detailed account of our earlier published *Brief Report* [8]. Here, we propose a simple model for the Landau-quantized 2DEG with a 1D periodic δ-modulation. A self-consistent field theory for calculating the absorption coefficient is presented. Our calculations show that the cyclotron mode in a Landau-quantized 2DEG is split into tunnelling-coupled modes in the weak-modulation limit. As the modulation potential is swept through the large intermediate-modulation regime, these two tunnelling-coupled modes gradually crossover into edge and 1D lattice magnetoplasmon modes in the strong-modulation limit.

The remainder of paper is organized as follows. In section 2, we present the numerical calculation of the energy eigenstates of a Landau-quantized 2DEG with 1D periodic δ-modulation. Section 3 is devoted to the calculation of the absorption coefficient in the mid-infrared regime. Section 4 contains numerical results for optical absorption with different parameters of potential strength and magnetic field. Section 5 contains a summary of key results and concluding remarks.

2. Numerical diagonalization for Landau states under 1D periodic δ-modulation

The single-particle Hamiltonian for a 2DEG in the x–y plane under a 1D periodic δ-modulation and a uniform perpendicular magnetic field B is, within the Landau gauge,

$$\mathcal{H}_0 = \frac{1}{2m^*}\left[-\hbar^2\frac{\partial^2}{\partial x^2} + \left(\frac{\hbar}{\mathrm{i}}\frac{\partial}{\partial y} + eBx\right)^2\right] + V(x) \tag{1}$$

where m^* is the electron effective mass. In (1), the 1D periodic δ-modulation potential $V(x)$ is chosen to be in the x direction and is given by

$$V(x) = \sum_{m=-\infty}^{\infty} V_m \delta(x - a_m) \tag{2}$$

where $V_m > 0$ denotes the repulsive modulation strength and a_m denotes the lattice site positions. We do not include the small effect of Coulomb interaction on the modulation potential.

In this periodic 1D δ-modulation potential, the Landau eigenstates of the original 2DEG are mixed, so we label the new single-particle energy eigenstates with quantum numbers (j, X_0) and use the Landau eigenstates as a basis set for the expansion

$$\psi_{j, X_0}(x, y) = \sum_{n=0}^{\infty} C_n(j, X_0)\, \phi_{n, X_0}(x, y) \tag{3}$$

where $\{C_n(j, X_0)\}$ are the expansion coefficients for the jth eigenstate. In (3), $\phi_{n, X_0}(x, y)$ are the harmonic oscillator wave functions for a homogeneous Landau-quantized 2DEG, given by

$$\phi_{n, X_0}(x, y) = \frac{1}{\sqrt{L_y}} \exp\left(\frac{iX_0 y}{L_H^2}\right) \varphi_{n, X_0}(x) \tag{4}$$

where L_y is the length of the sample along the y direction, $n = 0, 1, 2, \ldots$ is a Landau-level index, $X_0 = k_y L_H^2$ is the guiding centre, k_y is the wave vector along the y direction, and $L_H = (\hbar/eB)^{1/2}$ is the magnetic length. In (4), we have defined

$$\varphi_{n, X_0}(x) = \sqrt{\frac{1}{\pi^{1/2} 2^n n! L_H}} \exp\left[\frac{-(x + X_0)^2}{2L_H^2}\right] H_n\left(\frac{x + X_0}{L_H}\right) \tag{5}$$

where $H_n(x)$ is the nth-order Hermite polynomial. The expansion coefficient $C_n(j, X_0)$ in (3) can be decided from the following homogeneous linear equation:

$$\sum_{n=0}^{\infty} \left[\left(E_n^{(0)} - E_j(X_0)\right) \delta_{n, n'} + B_{n', n}(X_0)\right] C_n(j, X_0) = 0 \tag{6}$$

subject to the orthonormality condition:

$$\sum_{n=0}^{\infty} C_n(j, X_0) C_n(j', X_0) = \delta_{j, j'}.$$

Here, the energy eigenvalue in the absence of modulation is $E_n^{(0)} = (n + 1/2)\hbar\omega_c$, and $\omega_c = eB/m^*$ is the cyclotron frequency. Twenty Landau levels have been included in our numerical calculation. By setting the determinant of the coefficient matrix in (6) equal to zero, we obtain a secular equation for the new energy eigenvalues $E_j(X_0)$ in the presence of modulation. The Landau degeneracy with guiding centre X_0 is lifted by the 1D potential modulation. The second term in the coefficient matrix of (6) is defined as

$$B_{n', n}(X_0) = \sum_{l=-\infty}^{\infty} V_l \sqrt{\frac{1}{\pi 2^{(n+n')} n! n'! L_H^2}} \exp\left[\frac{-(a_l + X_0)^2}{L_H^2}\right] \times H_n\left(\frac{a_l + X_0}{L_H}\right) H_{n'}\left(\frac{a_l + X_0}{L_H}\right). \tag{7}$$

In (7), we have set

$$V_l = \begin{cases} V_e & \text{if } l \text{ is an even integer} \\ V_o & \text{if } l \text{ is an odd integer} \end{cases} \tag{8}$$

and

$$a_l = \begin{cases} la & \text{if } l \text{ is an even integer} \\ (l-1)a + \tau a & \text{if } l \text{ is an odd integer} \end{cases} \tag{9}$$

where $0 < \tau \leqslant 1$ measures the effect of a complex unit cell. Clearly, $B_{n',n}(X_0)$ has the periodicity of $2a$ in the 1D lattice as a function of X_0. From this, it follows from (6) that $E_j(X_0) = E_j(X_0 + 2a)$. Moreover, because the coefficient matrix in (6) is real and symmetric, $C_n(j, X_0)$ are real numbers.

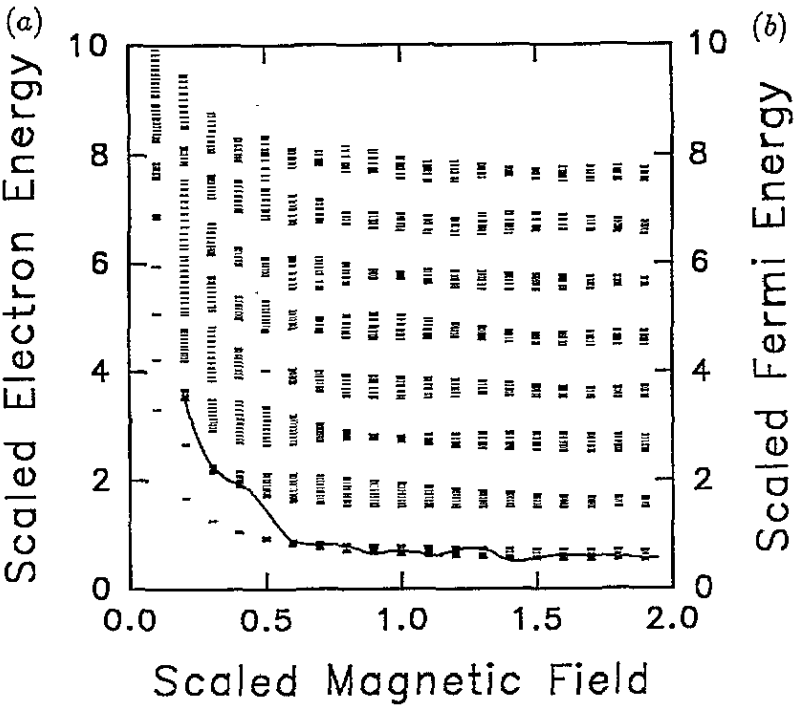

Figure 1. Plots of the scaled energy eigenvalues $E_j(X_0)/\hbar\omega_c$ (left-hand scale) and the scaled Fermi energy $E_F/\hbar\omega_c$ (solid curve with $n_{2D}a^2 = 1.0$ and right-hand scale) as a function of the scaled magnetic field $\Phi/\phi_0 = a^2/2\pi L_H^2$. The parameters used in the following numerical calculations are: $a = 1000$ Å, $m^* = 0.067m_e$, $\epsilon_b = 12.9$, $L_z = 50$ Å, $\gamma = 0.12$ meV, $T = 0$ K, $\tau = 1.0$, $B = 0.45$ T, $n_{2D}a^2 = 5.0$, $\bar{V} = (V_e/a)/(\sqrt{\pi}\hbar^2/m^*a^2) = (V_o/a)/(\sqrt{\pi}\hbar^2/m^*a^2) = 1.0$.

In figures 1 we present the magnetic field dependence of the scaled energy eigenvalues $E_j(X_0)/\hbar\omega_c$ (a) and the scaled Fermi energy $E_F/\hbar\omega_c$ (b) as a function of the dimensionless magnetic field parameter $\Phi/\phi_0 = a^2/2\pi L_H^2$ for the simple unit cell. Clearly from figure 1(a), the original Landau-level degeneracy with guiding centre X_0 is lifted due to the 1D potential modulation. Each Landau level is vertically expanded into a band. The bandwidth oscillates with magnetic field, indicating the suppression of electron tunnelling (zero bandwidth) in the system. The bandwidth also oscillates with band index and decreases at large magnetic fields. Different bands are found to overlap strongly at low magnetic fields. The electron energy is shifted upward and the electron eigenstates become bound states when

the magnetic field is weak. Figure 1(*b*) has steps as the magnetic field is varied. Each step corresponds to the depopulation of one band. In the high-magnetic-field limit, the Fermi energy is frozen in the lowest-energy band, signalling complete depopulation and the 1D extreme limit. However, at low magnetic fields, the Fermi energy is raised as a result of the decrease in the Landau-level degeneracy as the magnetic field is reduced.

At weak magnetic fields, the dispersion as a function of the guiding centre X_0/a is weak for the lower energy bands but it becomes strong for higher bands. The band gap becomes smaller and smaller for higher bands. When the magnetic field increases, the dispersion of the lower bands is enhanced.

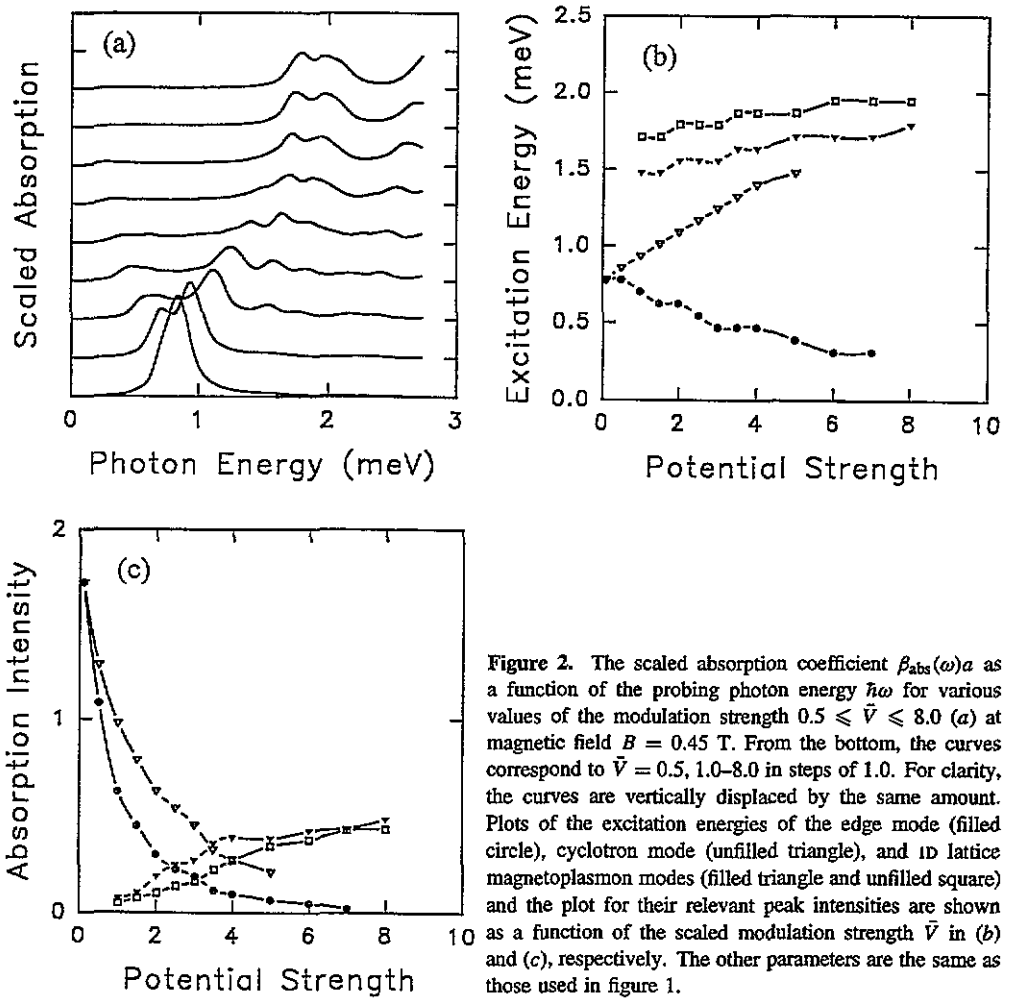

Figure 2. The scaled absorption coefficient $\beta_{abs}(\omega)a$ as a function of the probing photon energy $\hbar\omega$ for various values of the modulation strength $0.5 \leqslant \bar{V} \leqslant 8.0$ (*a*) at magnetic field $B = 0.45$ T. From the bottom, the curves correspond to $\bar{V} = 0.5$, 1.0–8.0 in steps of 1.0. For clarity, the curves are vertically displaced by the same amount. Plots of the excitation energies of the edge mode (filled circle), cyclotron mode (unfilled triangle), and 1D lattice magnetoplasmon modes (filled triangle and unfilled square) and the plot for their relevant peak intensities are shown as a function of the scaled modulation strength $\bar{V}$ in (*b*) and (*c*), respectively. The other parameters are the same as those used in figure 1.

3. Self-consistent field theory for the absorption coefficient

The induced part of the density matrix is calculated as

$$\langle jX_0 \left|\rho_1(r_{\|})\right| j'X_0'\rangle = \left(\frac{f_0\left[E_j(X_0) - E_F\right] - f_0\left[E_{j'}(X_0') - E_F\right]}{\hbar\omega + i\gamma - E_{j'}(X_0') + E_j(X_0)}\right) \langle jX_0 \left|H_1(r_{\|})\right| j'X_0'\rangle \quad (10)$$

where an x-direction-polarization probing field in the form of $\Phi^{\rm ext}(r_{||}, z)\exp(i\omega t)$ is assumed, $\langle r_{||}|jX_0\rangle \equiv \psi_{j,X_0}(r_{||}) = \psi_{j,X_0}(x, y)$, $E_j(X_0)$ is the single-particle energy, $f_0\left[E_j(X_0) - E_{\rm F}\right]$ is the Fermi–Dirac distribution function in equilibrium, $H_1(r_{||})$ is the induced part of the Hamiltonian, $E_{\rm F}$ is the Fermi energy which is determined by the doped electron density, ω is the frequency of the probing light, and γ stands for the optical broadening due to impurity, phonon and surface roughness scatterings. In the random-phase approximation, the induced electron density is written as

$$\begin{aligned} n_{\rm ind}(r_{||}, z; t) &= {\rm Tr}\left[\rho_1(r_{||}, z; t)\delta(r_{||} - r'_{||})\delta(z - z')\right] \\ &\equiv n_{\rm ind}(r_{||}; \omega)\,|\xi_0(z)|^2\,\exp\left[{\rm i}(\omega + {\rm i}\gamma/\hbar)t\right] \end{aligned} \tag{11}$$

where

$$\begin{aligned} n_{\rm ind}(r_{||}; \omega) &= 2\sum_{jX_0}\sum_{j'X'_0} \langle jX_0\left|\rho_1(r_{||})\right|j'X'_0\rangle\,\langle j'X'_0\left|\delta(r_{||} - r'_{||})\right|jX_0\rangle \\ &= 2\sum_{jX_0}\sum_{j'X'_0} \psi^*_{j'X'_0}(r_{||})\,\psi_{jX_0}(r_{||})\left(\frac{f_0\left[E_j(X_0) - E_{\rm F}\right] - f_0\left[E_{j'}(X'_0) - E_{\rm F}\right]}{\hbar\omega + {\rm i}\gamma - E_{j'}(X'_0) + E_j(X_0)}\right) \\ &\quad\times\left[-e\int {\rm d}r'_{||}\,{\rm d}z'\,|\xi_0(z')|^2\,\psi^*_{jX_0}(r'_{||})\,\psi_{j'X'_0}(r'_{||})\Phi^{\rm ext}(r'_{||}, z'; \omega)\right. \\ &\quad+\sum_q \frac{2\pi e^2}{\epsilon_{\rm s} q}\,n_{\rm ind}(q; \omega)\left(\int {\rm d}r'_{||}\,\exp(-{\rm i}q\cdot r'_{||})\,\psi^*_{jX_0}(r'_{||})\,\psi_{j'X'_0}(r'_{||})\right) \\ &\quad\left.\times\left(\int {\rm d}z'\,{\rm d}z''\,|\xi_0(z')|^2\,\exp(-q|z' - z''|)\,|\xi_0(z'')|^2\right)\right]. \end{aligned} \tag{12}$$

Here, $\epsilon_{\rm s} = 4\pi\epsilon_0\epsilon_{\rm b}$ with $\epsilon_{\rm b}$ being the average background dielectric constant. In (11), $\xi_0(z)$ stands for the envelope function in the z direction. Because the thickness of 2DEG layer is usually much smaller than the period of modulation, we assume that electrons are restricted to the lowest subband along the z direction. By noting that the wavelength of the probing field is much larger than the sample size, we neglect the variation in the amplitude of the perturbed field in the x–y plane. With these assumptions in mind and taking the probing light as polarized in the x direction, we write

$$\Phi^{\rm ext}(r'_{||}; \omega) \equiv \int {\rm d}z'\,|\xi_0(z')|^2\,\Phi^{\rm ext}(r'_{||}, z'; \omega) = -E_0^{\rm ext}x'. \tag{13}$$

For convenience, we introduced the following notation:

$$V(q) = \frac{2\pi e^2}{\epsilon_{\rm s} q}\int {\rm d}z'\,{\rm d}z''\,|\xi_0(z')|^2\,\exp(-q|z' - z''|)\,|\xi_0(z'')|^2 \tag{14}$$

$$F_{jX_0, j'X'_0}(q) = \int {\rm d}r'_{||}\,\exp(-{\rm i}q\cdot r'_{||})\,\psi^*_{jX_0}(r'_{||})\,\psi_{j'X'_0}(r'_{||}) \tag{15}$$

$$X_{jX_0, j'X'_0} = X_{jj'}(X_0)\,\delta_{X_0, X'_0} = \int {\rm d}r'_{||}\,\psi^*_{jX_0}(r'_{||})\,x'\,\psi_{j'X'_0}(r'_{||}) \tag{16}$$

$$U_{jX_0, j'X'_0}(\omega) = \sum_q V(q)\,F_{jX_0, j'X'_0}(q)\,n_{\rm ind}(q; \omega) \tag{17}$$

$$n_{\rm ind}(q'; \omega) = \frac{1}{A}\int {\rm d}r_{||}\,\exp({\rm i}q'\cdot r_{||})\,n_{\rm ind}(r_{||}; \omega) \tag{18}$$

where $A = L_x L_y$ is the sample area with L_x denoting the length of the sample in the x direction. Therefore, it is a simple matter to obtain the following self-consistent linear equation determining the screened Coulomb interaction matrix:

$$\sum_{jX_0}\sum_{j'X_0'}\left[\delta_{j,k}\delta_{j',k'}\delta_{X_0,Y_0}\delta_{X_0',Y_0'} - 2\left(\frac{f_0\left[E_j(X_0)-E_F\right]-f_0\left[E_{j'}(X_0')-E_F\right]}{\hbar\omega+i\gamma-E_{j'}(X_0')+E_j(X_0)}\right)\times\left(\frac{1}{A}\sum_{q'}F^*_{jX_0,j'X_0'}(q')\,F_{kY_0,k'Y_0'}(q')\,V(q')\right)\right]\left[\frac{U_{jX_0,j'X_0'}(\omega)}{eE_0^{ext}}\right] = S_{kY_0,k'Y_0'}(\omega) \tag{19}$$

where the source term is

$$S_{kY_0,k'Y_0'}(\omega) = 2\sum_{jX_0}\sum_{j'X_0'}\left(\frac{f_0\left[E_j(X_0)-E_F\right]-f_0\left[E_{j'}(X_0')-E_F\right]}{\hbar\omega+i\gamma-E_{j'}(X_0')+E_j(X_0)}\right)X_{jX_0,j'X_0'}\times\left(\frac{1}{A}\sum_{q'}F^*_{jX_0,j'X_0'}(q')\,F_{kY_0,k'Y_0'}(q')\,V(q')\right). \tag{20}$$

In order to obtain information concerning the oscillator strengths of the dipole-active excitation modes, we have to calculate the absorption coefficient as a function of the frequency ω. Further calculation shows that (15) is given by

$$F_{jX_0,j'X_0'}(q) = \delta_{X_0',X_0+q_yL_H^2}\,\exp\left[\frac{iq_x}{2}\left(2X_0+q_yL_H^2\right)\right]f_{j,j';X_0}(q) \tag{21}$$

where

$$f_{j,j';X_0}(q) = \sum_{nn'}C_n^*(j,X_0)\,C_{n'}(j',X_0+q_yL_H^2)\,\mathcal{L}_{nn'}(q) \tag{22}$$

and

$$\mathcal{L}_{nn'}(q) = \sqrt{\frac{N_<!}{N_>!}}\,i^{|n-n'|}\left[\frac{-(q_x+iq_y)}{q}\right]^{(n'-n)}\exp\left(\frac{-q^2L_H^2}{4}\right)\left(\frac{q^2L_H^2}{2}\right)^{|n-n'|/2}\times L_{N_<}^{(|n-n'|)}\left(\frac{q^2L_H^2}{2}\right). \tag{23}$$

In equation (23), $q = \sqrt{q_x^2+q_y^2}$, $N_< = \min(n,n')$, $N_> = \max(n,n')$, and $\mathcal{L}_n^m(x)$ is a Laguerre polynomial. The Fourier component of the induced polarization function is defined through

$$P_{ind}(\omega) = -e\int dr_{||}\,n_{ind}(r_{||};\omega)x\,. \tag{24}$$

Therefore, we obtain the Lorentz ratio $\alpha_L(\omega) \equiv P_{ind}(\omega)/E_0^{ext}$ of the induced polarization

$$\alpha_L(\omega) = -\frac{e^2A}{2\pi L_H^2}\sum_{j\neq j'}\int_0^{2a}\frac{dX_0}{a}\,X^*_{jj'}(X_0)\left(\frac{f_0\left[E_j(X_0)-E_F\right]-f_0\left[E_{j'}(X_0)-E_F\right]}{\hbar\omega+i\gamma-E_{j'}(X_0)+E_j(X_0)}\right)\times\left[X_{jj'}(X_0)+\sum_{m=-\infty}^{\infty}\left(\frac{n_{ind}(mG;\omega)}{eE_0^{ext}}\right)\times S(|mG|)F_{j,j';X_0}(mG)\exp(imGX_0)\right] \tag{25}$$

where the summation over m includes the contribution from Umklapp scattering, and $G = 2\pi/2a$ is a reciprocal-lattice vector. The dipole transition matrix $X_{jj'}(X_0)$ defined in (16) is calculated as

$$X_{jj'}(X_0) = \frac{L_H}{\sqrt{2}} \sum_{n=0}^{\infty} C_n(j, X_0)\left[\sqrt{n+1}C_{n+1}(j', X_0) + \sqrt{n}C_{n-1}(j', X_0)\right] - X_0\delta_{j,j'} \quad (26)$$

and the form factor in (25) is

$$F_{j,j';X_0}(mG) \equiv F_{jX_0,j'X_0'}(q_x = mG, q_y = 0)$$
$$= \sum_{nn'=0}^{\infty} C_n(j, X_0)C_{n'}(j', X_0)\left[\sqrt{\frac{N_<!}{N_>!}}\,(\mathrm{i}\,\mathrm{sgn}(-m))^{(N_>-N_<)}\exp\left(\frac{-m^2G^2L_H^2}{4}\right)\right.$$
$$\left.\times\left(\frac{m^2G^2L_H^2}{2}\right)^{(N_>-N_<)/2}\mathcal{L}_{N_<}^{(N_>-N_<)}\left(\frac{m^2G^2L_H^2}{2}\right)\right] \quad (27)$$

where $\mathrm{sgn}(x)$ is the signum function. If we employ the Fang–Howard variational type of envelope function for the lowest subband along the z direction, the form factor of the Coulomb interaction due to the finite thickness L_z of the EG layer has been calculated as

$$S(|mG|) = \frac{2\pi e^2}{\epsilon_s|m|G}\left[\frac{8+9|m|GL_z+3m^2G^2L_z^2}{8(1+|m|GL_z)^3}\right]. \quad (28)$$

The induced electron density in (25) is a solution of the following linear equation:

$$\sum_{m=-\infty}^{\infty}\left[\delta_{m',m} - A_{m',m}(\omega)\right]\left(\frac{n_{\mathrm{iad}}(mG;\,\omega)}{eE_0^{\mathrm{ext}}}\right) = R_{m'}(\omega) \quad (29)$$

which is a special case of the general result in (19) when we only include the dipole-active modes where

$$A_{m',m}(\omega) = \frac{1}{2\pi L_H^2}\sum_{j\neq j'}\int_0^{2a}\frac{\mathrm{d}X_0}{a}\,F^*_{j,j';X_0}(m'G)F_{j,j';X_0}(mG)S(|mG|)\exp[\mathrm{i}(m-m')GX_0]$$
$$\times\left(\frac{f_0\left[E_j(X_0)-E_F\right]-f_0\left[E_{j'}(X_0)-E_F\right]}{\hbar\omega+\mathrm{i}\gamma-E_{j'}(X_0)+E_j(X_0)}\right) \quad (30)$$

is part of the dielectric function matrix, and the source term is

$$R_m(\omega) = \frac{1}{2\pi L_H^2}\sum_{j\neq j'}\int_0^{2a}\frac{\mathrm{d}X_0}{a}\,F^*_{j,j';X_0}(mG)\exp(-\mathrm{i}mGX_0)X_{jj'}(X_0)$$
$$\times\left(\frac{f_0\left[E_j(X_0)-E_F)\right]-f_0\left[E_{j'}(X_0)-E_F\right]}{\hbar\omega+\mathrm{i}\gamma-E_{j'}(X_0)+E_j(X_0)}\right). \quad (31)$$

The absorption coefficient is related to the imaginary part of the Lorentz ratio in a straightforward way and the result is [15]

$$\beta_{\mathrm{abs}}(\omega) = \frac{\omega}{\epsilon_0 cL_z An(\omega)}\left[\rho_{\mathrm{ph}}(\omega)+1\right]\mathrm{Im}\,\alpha_L(\omega) \quad (32)$$

where $\rho_{ph}(\omega) = [\exp(\hbar\omega/k_BT)-1]^{-1}$ is the photon distribution function, and the frequency-dependent refractive index is found to be

$$n(\omega) = \left\{\frac{1}{2}\left[\left(\epsilon_b + \frac{\mathrm{Re}\,\alpha_L(\omega)}{\epsilon_0 L_z A}\right) + \sqrt{\left(\epsilon_b + \frac{\mathrm{Re}\,\alpha_L(\omega)}{\epsilon_0 L_z A}\right)^2 + \left(\frac{\mathrm{Im}\,\alpha_L(\omega)}{\epsilon_0 L_z A}\right)^2}\right]\right\}^{1/2}. \tag{33}$$

From (33), we know that the dipole-active mode in this system is the one with $q_y = 0$, i.e., the guiding centre remains unchanged during the electron transitions.

We easily obtain the equation determining the magnetoplasmon excitation energies from (29) by setting $\gamma = 0$, and the result is

$$\det\left[\delta_{m',m} - A_{m',m}(\omega)\right] = 0. \tag{34}$$

Furthermore, after we invert the matrix in (29), we obtain the Fourier component of the induced electron density. Using these results, we can write the induced-electron-density distribution function in real space as

$$\begin{aligned} n_{ind}(r_{||};\,\omega) = {} & \frac{eE_0^{ext}L_y a}{2\pi L_H^2}\sum_{k=-\infty}^{+\infty}\sum_{j\neq j'}\int_0^{2a}\frac{dX_0}{a}\,\psi^*_{j',X_0+k2a}(r_{||})\,\psi_{j,X_0+k2a}(r_{||}) \\ & \times\left(\frac{f_0\left[E_j(X_0)-E_F\right]-f_0\left[E_{j'}(X_0)-E_F\right]}{\hbar\omega+i\gamma-E_{j'}(X_0)+E_j(X_0)}\right) \\ & \times\left[X_{jj'}(X_0)+\sum_{m=-\infty}^{\infty}\left(\frac{n_{ind}(mG;\,\omega)}{eE_0^{ext}}\right)\right. \\ & \left.\times S(|mG|)F_{j,j';X_0}(mG)\,\exp(imGX_0)\right] \end{aligned} \tag{35}$$

which is obviously periodic in the x direction. Therefore, the gauge invariance is retained in the physically measurable quantity although we have chosen the asymmetric *Landau gauge*.

4. Numerical results for the absorption coefficient

Figures 2 display the scaled absorption coefficient for the simple unit cell as a function of probing photon energy for different values of modulation strength. These plots show the resonant peak positions and the intensities of the absorption coefficient as a function of the modulation strength. From figure 2(*a*), we can clearly see how the magnetoplasmon mode changes from a cyclotron mode in the weak-modulation regime (single peak at $\bar{V} = (V_e/a)/(\sqrt{\pi}\hbar^2/m^*a^2) = (V_o/a)/(\sqrt{\pi}\hbar^2/m^*a^2) = 0.5$) to a 1D lattice magnetoplasmon mode when the modulation is strong (a series of peaks at $\bar{V} = 8.0$). However, for intermediate modulation potentials, the cyclotron mode splits into two new tunnelling-coupled modes. As the modulation strength increases, one of these coupled modes gradually changes into a 1D lattice magnetoplasmon mode while the other one develops into an edge mode. The repulsive potential first shifts the electron energy upward which enhances the electron tunnelling at both sides of the scatterer. However, when the modulation is sufficiently strong that the electron tunnelling is suppressed, we are left with a 1D array of isolated quantum wires. The peak becomes broadened and the weight of the spectrum is distributed more extensively. Figure 2(*b*) shows that the potential strength dispersion of the excitation energy of tunnelling-coupled modes is appreciable compared with the

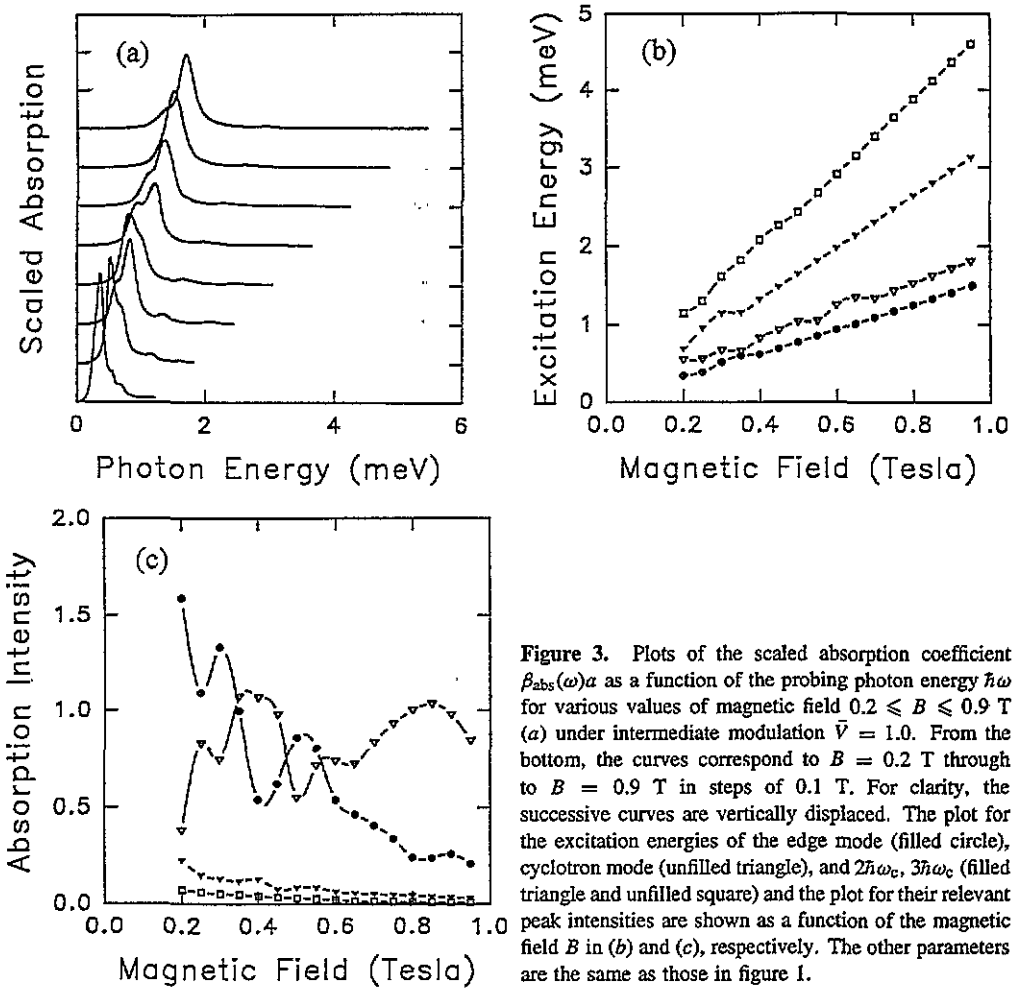

Figure 3. Plots of the scaled absorption coefficient $\beta_{abs}(\omega)a$ as a function of the probing photon energy $\hbar\omega$ for various values of magnetic field $0.2 \leqslant B \leqslant 0.9$ T (a) under intermediate modulation $\bar{V} = 1.0$. From the bottom, the curves correspond to $B = 0.2$ T through to $B = 0.9$ T in steps of 0.1 T. For clarity, the successive curves are vertically displaced. The plot for the excitation energies of the edge mode (filled circle), cyclotron mode (unfilled triangle), and $2\hbar\omega_c$, $3\hbar\omega_c$ (filled triangle and unfilled square) and the plot for their relevant peak intensities are shown as a function of the magnetic field B in (b) and (c), respectively. The other parameters are the same as those in figure 1.

1D lattice magnetoplasmon modes. When the repulsive potential becomes strong, a hard potential wall is formed which favours the electrons performing skipping orbits along the walls. As a consequence, the excitation energy of an edge mode decreases as the potential increases. In the weak-potential regime, the tunnelling-coupled modes are the dominant excitations, whereas in the strong-potential regime, the 1D lattice magnetoplasmon mode becomes dominant. This behaviour is verified in figure 2(c) where the scaled peak intensities are shown as a function of the potential strength for different modes. There is a crossover region where the absorption peak intensities of both the tunnelling-coupled and 1D lattice magnetoplasmon modes are comparable. At some critical value of modulation strength, the cyclotron-like mode ceases to exist and only the edge mode is left. The intensity of an edge mode at strong modulations becomes too weak and invisible. Therefore, the whole system only displays the behaviour of 1D lattice magnetoplasmon modes in the strong-modulation limit as for a 1D array of quantum wires.

Figures 3 are the plots of scaled absorption coefficient for the simple unit cell as a function of the probing photon energy for various values of the magnetic field in the intermediate-modulation regime and the plots for magnetic field dispersions of peak positions

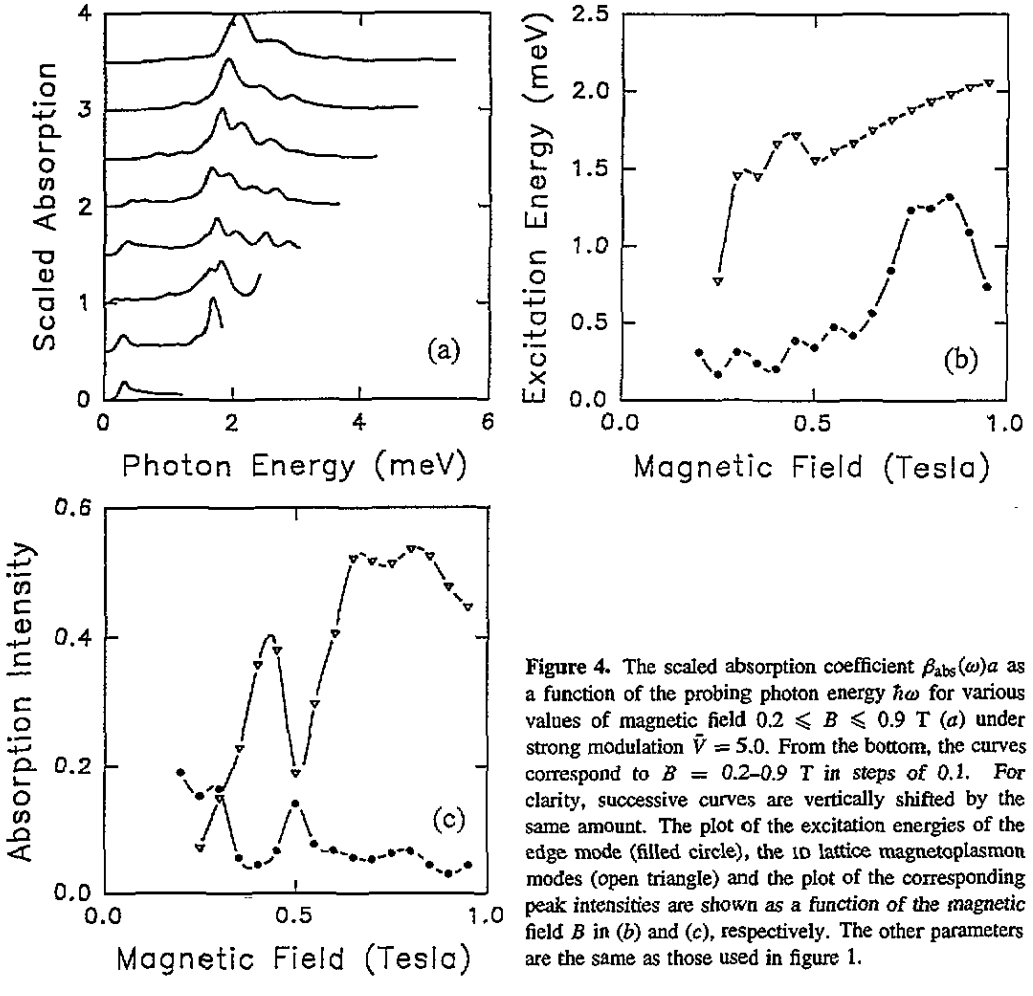

Figure 4. The scaled absorption coefficient $\beta_{abs}(\omega)a$ as a function of the probing photon energy $\hbar\omega$ for various values of magnetic field $0.2 \leqslant B \leqslant 0.9$ T (a) under strong modulation $\tilde{V} = 5.0$. From the bottom, the curves correspond to $B = 0.2$–0.9 T *in steps of 0.1*. For clarity, successive curves are vertically shifted by the same amount. The plot of the excitation energies of the edge mode (filled circle), the 1D lattice magnetoplasmon modes (open triangle) and the plot of the corresponding peak intensities are shown as a function of the magnetic field B in (b) and (c), respectively. The other parameters are the same as those used in figure 1.

and intensities. From figure 3(a), we find the emergence of tunnelling-coupled modes into a cyclotron mode in the strong magnetic field (single peak at $B = 0.9$ T). During this procedure, there are fast interchanges of peak intensity between two tunnelling-coupled modes with the increase of the magnetic field. The $2\hbar\omega_c$ and $3\hbar\omega_c$ resonances are greatly suppressed at strong magnetic fields. The magnetic field dispersion of the excitation energies in figure 3(b) shows us the crossover behaviour from the weak- to strong-magnetic-field regimes. The linear dispersion of all the modes is recovered at strong magnetic fields. However, as magnetic field decreases, the excitation energies are found to oscillate with field. The strong oscillations in the tunnelling-coupled modes can extend over to high magnetic fields. The visible $2\hbar\omega_c$ and $3\hbar\omega_c$ modes at low magnetic fields are the consequence of the breaking of translational symmetry by the 1D potential modulation in the system. Figure 3(c) demonstrates the interchanges of the scaled peak intensity of the tunnelling-coupled modes as the magnetic field is varied. There are significant peak strength exchanges across the whole intermediate-field regime which correspond to a series of anti-phase oscillations in the peak strengths as a function of the magnetic field for these two modes. The peak intensities of tunnelling-coupled modes are found to be much larger than those of $2\hbar\omega_c$

and $3\hbar\omega_c$ modes. At strong magnetic fields, one of the tunnelling-coupled modes evolves into an edge mode and the peak intensity of it decreases greatly with the increase of the magnetic field— whereas the peak intensity of a cyclotron-like mode which is also split out from the tunnelling-coupled modes increases with magnetic field in an oscillating way.

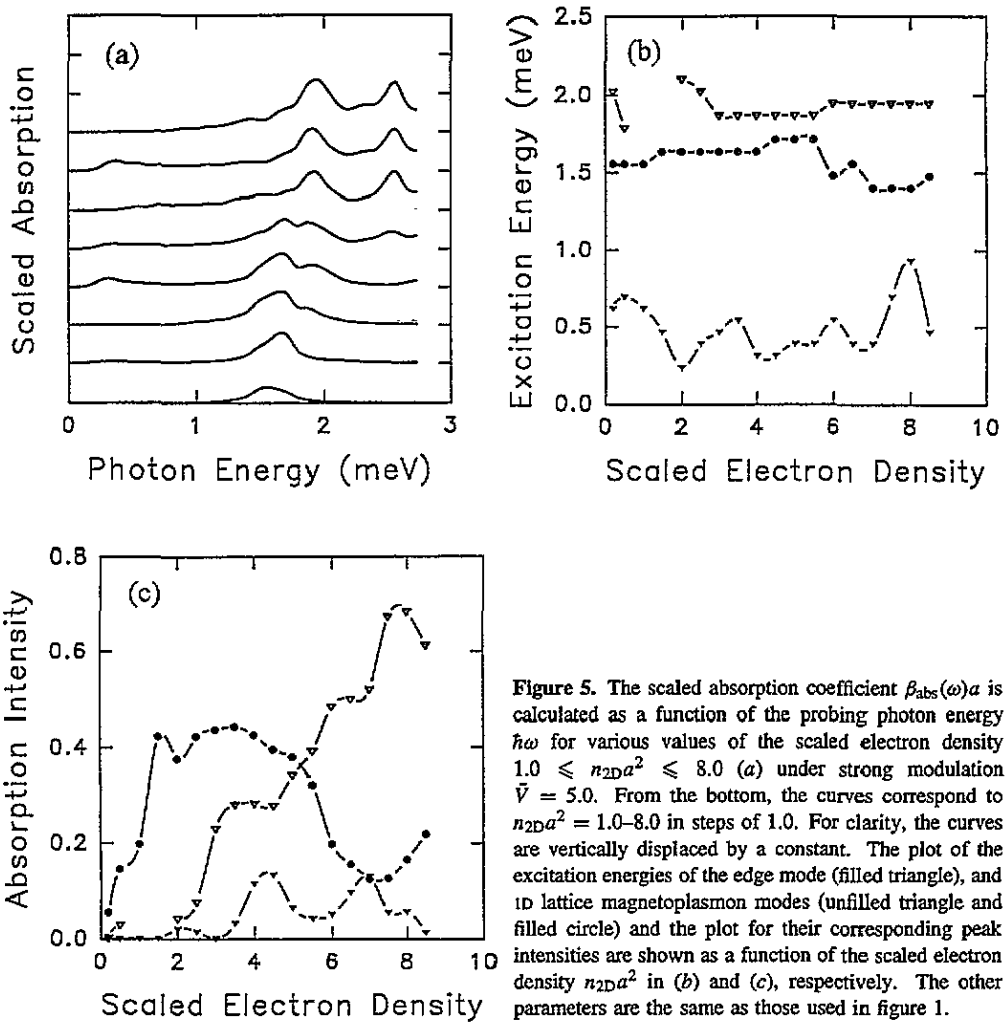

Figure 5. The scaled absorption coefficient $\beta_{abs}(\omega)a$ is calculated as a function of the probing photon energy $\hbar\omega$ for various values of the scaled electron density $1.0 \leqslant n_{2D}a^2 \leqslant 8.0$ (*a*) under strong modulation $\tilde{V} = 5.0$. From the bottom, the curves correspond to $n_{2D}a^2 = 1.0$–8.0 in steps of 1.0. For clarity, the curves are vertically displaced by a constant. The plot of the excitation energies of the edge mode (filled triangle), and 1D lattice magnetoplasmon modes (unfilled triangle and filled circle) and the plot for their corresponding peak intensities are shown as a function of the scaled electron density $n_{2D}a^2$ in (*b*) and (*c*), respectively. The other parameters are the same as those used in figure 1.

As a comparison with figure 3, we show in figures 4 plots of the scaled absorption spectra for the simple unit cell in the strong-modulation regime as a function of the probing photon energy at different values of the magnetic field. We also show plots for the magnetic field dispersions of both the peak positions and the intensities in this case. If we start from edge and 1D magnetoplasmon modes at $B = 0.2$T, the emergence of these two modes into a cyclotron mode in figure 4(*a*) occurs at even higher magnetic fields ($B > 0.9$T), passing through the formation of tunnelling-coupled modes. Increasing the magnetic field first enhances the electron tunnelling via the formation of two tunnelling-coupled modes, and then the magnetic field further suppresses the electron tunnelling via the combining of these two modes into one cyclotron mode. The magnetic field dispersion of the excitation energies of tunnelling-coupled modes is shown in figure 4(*b*) displaying the whole evolution process of the normal modes. As the magnetic field is varied, the excitation energies of

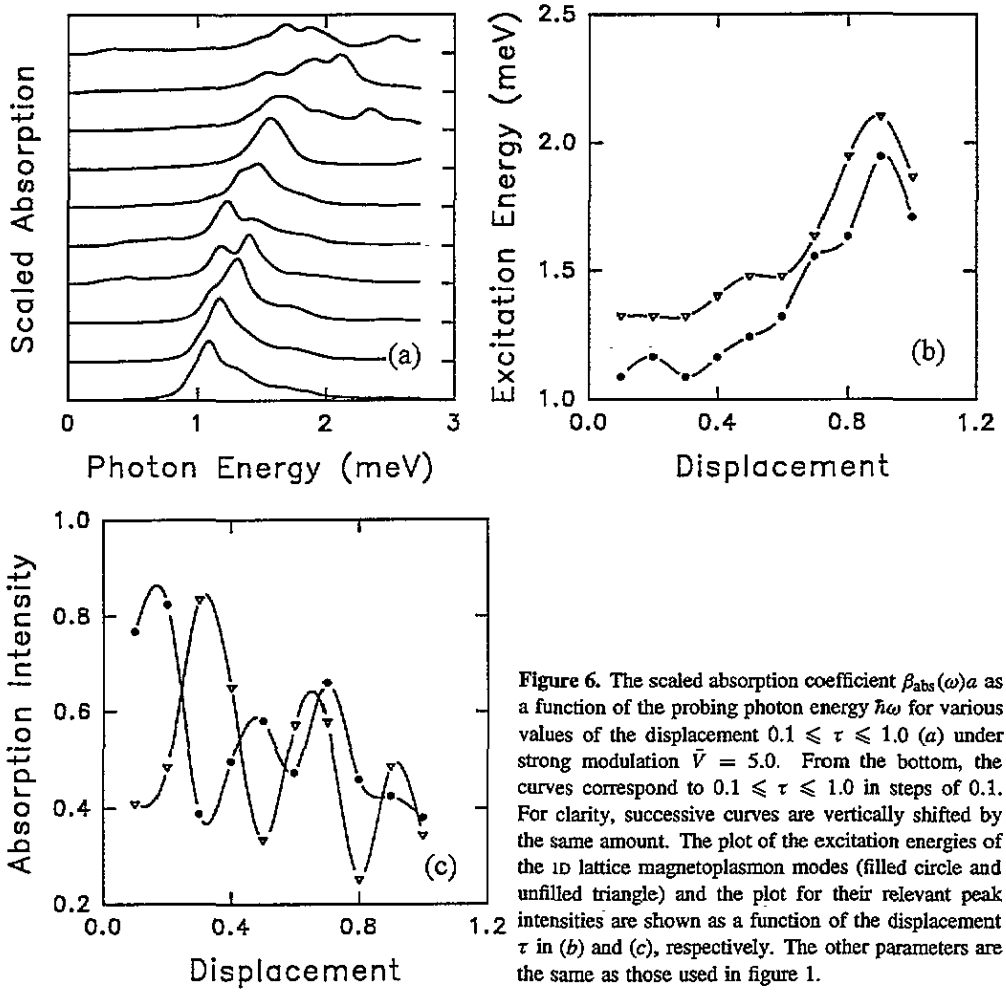

Figure 6. The scaled absorption coefficient $\beta_{abs}(\omega)a$ as a function of the probing photon energy $\hbar\omega$ for various values of the displacement $0.1 \leqslant \tau \leqslant 1.0$ (a) under strong modulation $\bar{V} = 5.0$. From the bottom, the curves correspond to $0.1 \leqslant \tau \leqslant 1.0$ in steps of 0.1. For clarity, successive curves are vertically shifted by the same amount. The plot of the excitation energies of the 1D lattice magnetoplasmon modes (filled circle and unfilled triangle) and the plot for their relevant peak intensities are shown as a function of the displacement τ in (b) and (c), respectively. The other parameters are the same as those used in figure 1.

these two modes are found to oscillate with the field strength. The large oscillations in the energy of the edge mode survive for higher magnetic fields and finally die out at very strong magnetic fields. On the other hand, the 1D lattice magnetoplasmon mode very quickly changes to a cyclotron mode and recovers to the linear dispersion relation at strong magnetic fields. Figure 4(c) demonstrates the oscillations in the scaled peak intensities of the edge and 1D lattice magnetoplasmon modes. The peak intensity of the edge mode decreases with magnetic field and is found to be always smaller than that of the 1D lattice magnetoplasmon mode except at very low magnetic fields. The oscillations in the peak intensities of these two modes are obviously out of phase. Although at high magnetic fields, the dispersion of the excitation energy for the 1D lattice magnetoplasmon mode already exhibits a linear relation, the intensity of this mode still sharply changes with magnetic field.

In figure 5, we calculate the absorption coefficient as a function of the probing photon energy in the strong-modulation regime, for the simple unit cell and various values of the electron density. We also plot the peak positions and the absorption intensities as functions of the electron density. Beginning as an edge and 1D lattice magnetoplasmon mode in figure 5(a), the 1D lattice magnetoplasmon mode bifurcates when the electron density increases,

while the peak position and intensity of the edge mode are oscillatory. From figure 5(*b*), it is evident that the excitation energy of the edge mode oscillates strongly with the electron density, i.e. the Fermi energy. When the Fermi energy lies about half-way between two bands, corresponding to localized states, the excitation energy has a minimum. In this case, the potential wall produced by strong modulation is comparatively hard which gives rise to the skipping motion of electrons. When the Fermi energy lies within the band, corresponding to extended states, the excitation energy of an edge mode has a maximum value. In this case, the potential wall becomes soft and the coupling between the two sides of the scatterer shifts the excitation energy upward. There are no oscillations in the excitation energies of the 1D lattice magnetoplasmon modes. Figure 5(*c*) presents the peak intensities of the edge and 1D lattice magnetoplasmon modes as a function of the electron density. The intensities of the two 1D lattice magnetoplasmon modes are always stronger than for the edge mode. There is a strong interchange of the two peak intensities which oscillate out of phase with the electron density. The peak intensity of the edge mode also oscillates with electron density in a way correlated with its excitation energy.

In figure 6, we plot the absorption coefficient for the complex unit cell as a function of the probing photon energy for various values of the displacement τ in the strong-modulation regime. We also plot the displacement dispersions of the peak positions and the intensities. In figure 6(*a*), the absorption coefficient is a periodic function of τ with the periodicity of $\tau \to 2-\tau$ when $0 < \tau \leqslant 1$. The small value $\tau = 0.1$ corresponds to the case with adjacent narrow and wide quantum wires in a unit cell, while the large value $\tau = 1$ corresponds to the quantum wires having equal width. There is a continuous crossover from a double-wire complex unit cell to a simple unit cell composed of only one wire. When τ is small, the absorption spectrum is dominated by the low-energy excitations inside the wide wire. There are strong peak intensity exchanges throughout the process. The peak is broadened when τ is increased. Our calculated results in figure 6(*b*) show that the excitation energies of the 1D lattice magnetoplasmon modes oscillate with τ and become large as τ is increased. The excitation energies also have a periodicity of $\tau \to 2 - \tau$ when $0 < \tau \leqslant 1$. The peak intensities of these two modes in figure 6(*c*) display strong anti-phase oscillations as a function of τ. With the increase of τ, the intensities of these two modes decrease and have periodicity satisfying $\tau \to 2 - \tau$ when $0 < \tau \leqslant 1$.

5. Concluding remarks and summary

In this paper, we used a 1D periodic δ-modulation to simulate a 1D array of quantum wires for simple and complex unit cells. The exact energy eigenstates were obtained by employing a numerical diagonalization method. On the basis of these results, we have derived a self-consistent field theory for the mid-infrared absorption coefficient of the system. The crossover from a cyclotron mode to two tunnelling-coupled modes and finally to edge and 1D lattice magnetoplasmon modes as the modulation strength is increased is thoroughly studied. The magnetic-field-enhanced and magnetic-field-suppressed electron tunnelling is associated with the evolution to cyclotron modes at strong magnetic fields passing through the formation of tunnelling-coupled modes. The edge mode excitation energy oscillates as a function of the electron density. These oscillations correspond to a soft or hard potential wall for which the electron states are extended or localized, respectively. The displacement dependencies of 1D lattice magnetoplasmon modes under strong modulation are found to be periodic, and correspond to the evolution from a complex unit cell which is composed of two quantum wires, one narrow and one wide, to a simple unit cell containing only one quantum wire.

Our preliminary calculations for the magnetoplasmon excitation in this 1D array of quantum wires has revealed some interesting features in the mid-infrared-range absorption spectrum for different values of modulation strength, magnetic field, electron density, and displacement. This work for the intermediate-modulation regime is complementary to previous studies for the weak- or strong-modulation limit. We expect that the present system will also show some interesting features in the magnetoresistance and Hall resistance if the modulation strength is chosen in the crossover regime. Calculations related to this problem are currently being done. We hope that this work will generate experimental interest in verifying the predictions in this paper.

Acknowledgments

The authors gratefully acknowledge the support in part from the City University of New York PSC-CUNY-BHE, grant No 662505, and the Office of Naval Research under Contract N00014-93-1-0576. We benefited from comments made by H L Cui, A H MacDonald, M Pepper and S E Ulloa.

References

[1] von Klitzing K, Dorda G and Pepper M 1980 *Phys. Rev. Lett.* **45** 494
[2] Tsui D C, Störmer H L and Gossard A C 1982 *Phys. Rev. Lett.* **48** 1559
[3] Weiss D, Richter K, Menschig A, Bergmann R, Schweizer H, von Klitzing K and Weimann G 1993 *Phys. Rev. Lett.* **70** 4118
[4] Alves E S, Beton P H, Henini M, Eaves L, Main P C, Hughes O H, Toombs G A, Beaumon S P and Wilkinson C D W 1989 *J. Phys.: Condens. Matter* **1** 8257
[5] Huang D and Gumbs G 1993 *Phys. Rev.* B **48** 2835
Huang D, Gumbs G and MacDonald A H 1993 *Phys. Rev.* B **48** 2843
[6] Středa P and MacDonald A H 1990 *Phys. Rev.* B **41** 11 892
[7] Weiss D, von Klitzing K, Ploog K and Weimann G 1989 *Europhys. Lett.* **8** 179
See also
Landwehr G (ed) 1989 *High Magnetic Fields in Semiconductor Physics II (Springer Series in Solid State Sciences 87)* (Berlin: Springer) p 357
[8] Huang D, Gumbs G and Horing N J M 1994 *Phys. Rev.* B **49** 11 463
[9] Hansen W, Horst M, Kotthaus J P, Merkt U, Sikorski C and Ploog K 1987 *Phys. Rev. Lett.* **58** 2586
[10] Wulf U, Kučera J and MacDonald A H 1993 *Phys. Rev.* B **47** 1675
[11] Smith C G, Pepper M, Newbury R, Ahmed H, Hasko D G, Peacock D C, Frost J E F, Ritchie D A, Jones G A C and Hill G 1990 *J. Phys. Condens. Matter* **2** 3405
Smith C G, Chen W, Pepper M, Ahmed H, Hasko D G, Ritchie D A, Frost J E F and Jones G A C 1992 *J. Vac. Sci. Technol.* B **10** 2904
[12] Gerhardts R R, Weiss D and von Klitzing K 1989 *Phys. Rev. Lett.* **62** 1173
Gerhardts R R and Zhang C 1990 *Phys. Rev. Lett.* **64** 1473
[13] Vasilopoulos P and Peeters F M 1989 *Phys. Rev. Lett.* **63** 2120
[14] Cui H L, Fessatidis V and Horing N J M 1989 *Phys. Rev. Lett.* **63** 2598
[15] Haug A 1972 *Theoretical Solid State Physics* vol 1 (New York: Pergamon) p 360